The Astrophysical Journal, 640:1135–1141, 2006 April 1

THE 2003 OCTOBER–NOVEMBER FAST HALO CORONAL MASS EJECTIONS AND THE LARGE-SCALE MAGNETIC FIELD STRUCTURES

Y. Liu[1] and K. Hayashi[1]

Received 2005 July 25; accepted 2005 December 1

ABSTRACT

The coronal magnetic field, computed from synoptic maps of the magnetic field and a potential field source surface (PFSS) model, reveals special configurations related to the active regions that were associated with most, if not all, fast halo coronal mass ejections (CMEs) in 2003 October–November. It was shown that these active regions emerged in an open field area, produced a large open field area after emerging, or sat on a boundary of two open field areas with the same polarity. This type of boundary is also known as a "plasma sheet." Such magnetic structures appear to be favorable for the propagation of the disturbance. MHD simulations were performed here to explore the behavior of the propagation of the disturbance against these special configurations of the background magnetic field. It is demonstrated that without the presence of open flux, the speed of the CMEs would have been only 78% of that with open flux present. It is also found that the CMEs from a heliospheric current sheet have a speed only 67% of the CMEs' speed from a plasma sheet, the source boundary with the same polarity.

Subject headings: Sun: activity — Sun: coronal mass ejections (CMEs) — Sun: magnetic fields

1. INTRODUCTION

The solar events in 2003 October–November, with their high rate of occurrence, extreme energetics, and the significance of the consequent geospace effects, have attracted much attention in the solar, space, and geomagnetic communities, leading to an intense study from fairly wide aspects to understand the events in the frame of the Sun-Earth connection (see, e.g., Gopalswamy et al. 2005a, 2005b and references therein), as well as the properties of their solar origins.

Most events in this period initiated from several active regions (see, e.g., Gopalswamy et al. 2005c). Special observations were arranged to observe these active regions. For example, Xu et al. (2004) and Yang et al. (2004) reported the successful observation of the October 29 X10 flare in the near-infrared continuum at 1.56 μm; Metcalf et al. (2005) measured the vector magnetic field of AR 10486 on the chromosphere, which produced the October 28 and 29 events. They further found that this region possessed an unusually large amount of free magnetic energy.

Gopalswamy et al. (2005c) suggested a link between the extreme characteristics of these events and the properties of the related active regions. Using statistical results of normal solar events as a reference, they demonstrated extreme properties of these events in terms of the coronal mass ejections (CMEs) being much faster, wider, and more energetic, having a much higher rate of occurrence of halo CMEs, being highly geoeffective, and being associated with large solar energetic particle events. They then showed that these properties "were commensurate with the size and energy of the associated active regions." They finally argued that such properties of active regions appear to be related to the X-ray flare size. This result is consistent with several recent studies that have suggested that the accelerations of the flare-related CMEs are probably determined by the magnitudes of the associated flares and/or the rate of the magnetic reconnection during flares (see, e.g., Moon et al. 2002; Cheng et al. 2003; Zhang et al. 2004; Qiu et al. 2004; Jing et al. 2005).

To our knowledge, no research has been carried out so far to analyze in detail the structures of the large-scale solar magnetic fields involved in these events. Since CMEs are believed to be related to the large-scale magnetic field but the flares related to the localized field, interaction between the large-scale and small-scale fields must occur. In addition, because the eruptions eventually propagate into interplanetary space, the magnetic field in the corona and heliosphere must be involved in the process of propagation. Therefore, it is reasonable to speculate that while a flare's characteristics define the representative speed of a flare-related CME in the first place, as addressed by many studies mentioned above, it is possible that the large-scale field overlying the flare areas may also work as a secondary factor to influence the speed when the disturbance propagates. It is thus worthwhile to characterize the large-scale magnetic fields associated with the fast halo CMEs in 2003 October–November in particular and discuss any roles such structures play in shaping the CMEs' speed, therefore functioning as an additional factor to ensure a high speed for the fast CMEs during their propagation. This is the purpose of this work. The reasons we only choose fast halo CMEs for this study are that (1) it is difficult to unambiguously identify the roles of the background fields for the slow CMEs because their low speeds may be due to the nature of either the flares or the background fields or a comprehensive effect from both. (It is not likely that all slow CMEs are caused by background fields possessing structures that are not favorable for propagation. If a flare already gives the associated CME a low speed in the first place, this CME is likely to become a slow CME, even though the background field favors propagation.) (2) The modeled coronal/heliospheric fields are more reliable because the solar origins of most halo CMEs are close to solar disk center, where the magnetic field measurement is more accurate than that near the limb.

We calculate coronal/heliospheric magnetic fields from synoptic maps of the magnetic field based on a potential field source surface (PFSS) model and use this calculation to analyze the large-scale magnetic field structures. The PFSS model, proposed thirty years ago and subsequently used by many researchers, has been proven to be fairly successful in modeling the large-scale magnetic field in the corona and heliosphere, determining the heliospheric current sheets and coronal holes, predicting the

[1] W. W. Hansen Experimental Physics Laboratory, Stanford University, 455 Via Palou, Stanford, CA 94305-4085.

TABLE 1
THE FAST HALO CMES IN 2003 OCTOBER–NOVEMBER

Event (1)	CME Date (2)	Time[a] (UT) (3)	Velocity (km s^{-1}) (4)	Class (5)	Flare Location (deg) (6)	Time[b] (UT) (7)	NOAA AR (8)
1.....	2003 Oct 21	03:54	1484	...	...	...	10486
2.....	2003 Oct 23	08:54	1406	X5.4/1B	S21 E88	08:24	10486
3.....	2003 Oct 24	02:54	1055	M7.6/1N	S19 E72	02:22	10486
4.....	2003 Oct 26	06:54	1371	X1.2/3B	S15 E44	06:17	10486
5.....	2003 Oct 26	17:54	1537	X1.2/1N	N02 W38	17:21	10484
6.....	2003 Oct 27	08:30	1322	M2.7/2F	N00 W45	07:46	10484
7.....	2003 Oct 28	11:30	2459	X17/4B	S16 E08	11:10	10486
8.....	2003 Oct 29	20:54	2029	X10/2B	S15 W02	20:49	10486
9.....	2003 Nov 02	17:30	2598	X8/2B	S14 W56	17:25	10486
10.....	2003 Nov 04	12:06	1208	C6	...	11:15	10486
11.....	2003 Nov 04	19:54	2657	X28/3B	S19 W89	19:32	10486
12[c]	2003 Nov 11	13:54	1315	M1/SF	S03 W61	13:35	10498
13.....	2003 Nov 18	08:50	1660	M4	...	08:12	10501

[a] The time when the CME is seen in the LASCO observation.
[b] Flare start time from Solar-Geophysical Data (2003 October–November).
[c] Determination of this event was from the CME catalog at http://cdaw.gsfc.nasa.gov/CME_list/ generated and maintained by S. Yashiro and G. Michalek at the Catholic University of America.

solar wind speed and interplanetary magnetic field, and many other applications (see, e.g., Schatten et al. 1969; Altschuler & Newkirk 1969; Hoeksema et al. 1982; Wang & Sheeley 1990, 1992; Wang 1993; Arge & Pizzo 2000; Schrijver & DeRosa 2003; Zhao & Webb 2003). In this model, it is assumed that the magnetic field is potential everywhere between the photosphere and a spherical source surface. The modeled field matches the radial component on the photosphere and is forced to become purely radial on the source surface.

We start, in § 2, with a list of the fast halo (including full and partial) CMEs in 2003 October–November and then present the evolution of the active regions during this period. In § 3, the magnetic field structures computed from the PFSS model are analyzed in terms of the locations of the fast halo CMEs and the active regions. MHD simulations are performed in § 4 to study the characteristics of the disturbance propagation against different configurations of the background magnetic field. We give our conclusions in § 5.

2. OBSERVATIONS

Listed in Table 1 are the fast halo CMEs in 2003 October–November chosen under the following criteria: (1) they are full or partial halo CMEs, (2) they have a speed greater than 1000 km s^{-1}, and (3) the solar source regions are determined. All the CMEs except event 12 were from Gopalswamy et al. (2005c). Determination of event 12 was from the CME catalog generated and maintained by S. Yashiro and G. Michalek at the Catholic University of America.[2] Other parameters of the CMEs, such as time and speed, were also from this catalog. Column (1) of Table 1 is the event identification number. Columns (2)–(4) describe the date, time, and speed of the CME, respectively. Information on related flares is presented in columns (5)–(7). Column (8) denotes the active region that was identified to be associated with the CME. It is seen that these fast halo CMEs were actually associated with four active regions: AR 10484, 10486, 10498, and 10501.

We present in Figure 1 the synoptic maps of the magnetic field for four successive solar rotations from 2003 August to

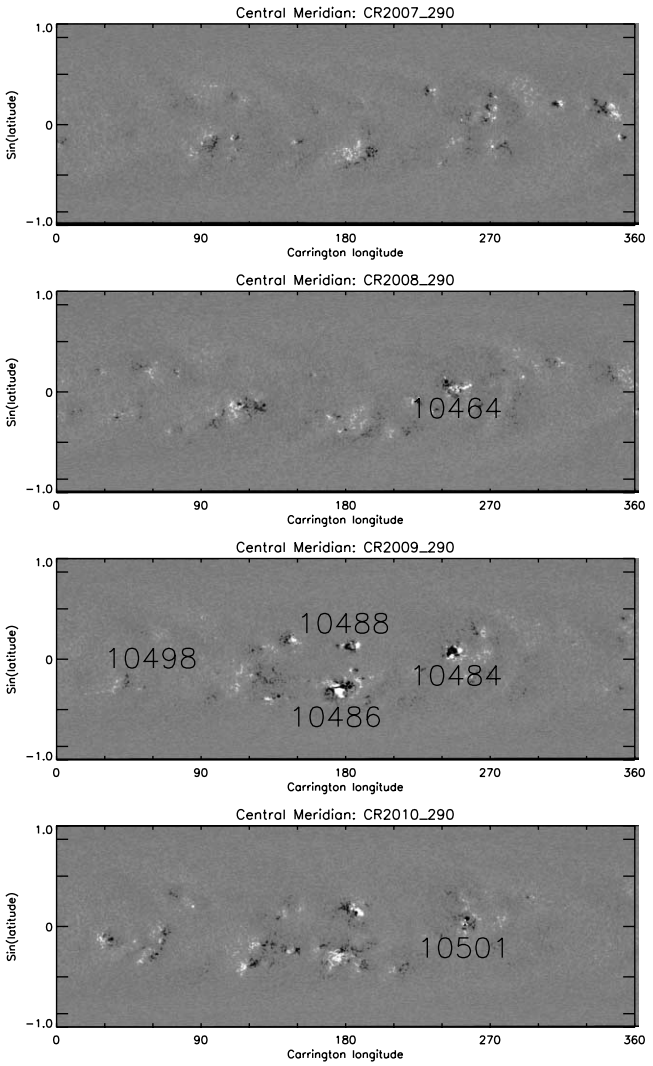

FIG. 1.—Synoptic maps of the magnetic field for four successive solar rotations. The central meridian passage dates of the maps are, from top to bottom, September 4, October 1, October 28, and November 25. The magnetic field data were taken by the Michelson Doppler Imager (MDI) aboard *SOHO*.

[2] Available at http://cdaw.gsfc.nasa.gov/CME_list/.

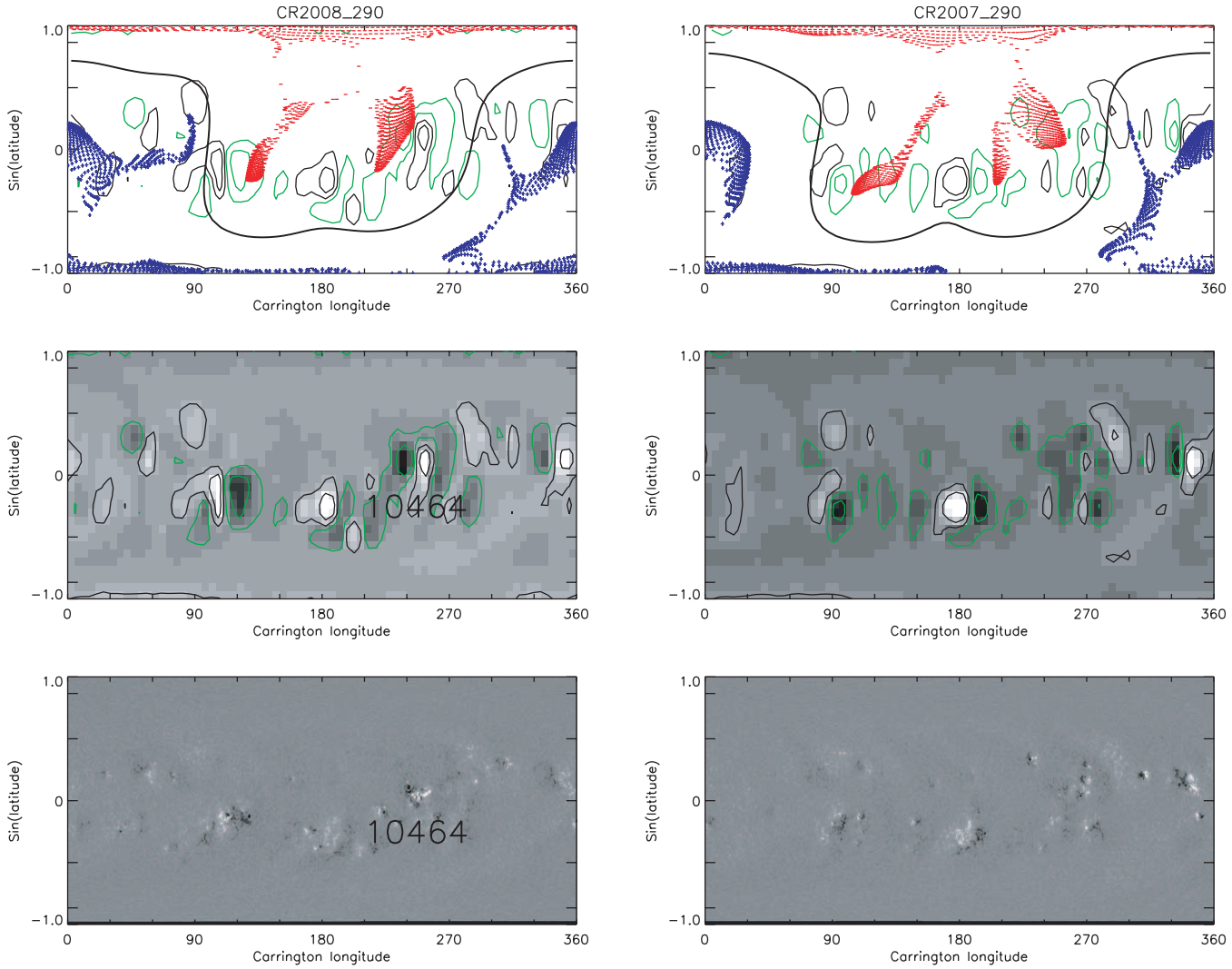

FIG. 2.—Synoptic maps of the magnetic field and the coronal field structures for the second (*left*) and the third (*right*) rotations of Fig. 1. The magnetic field data were taken by the MDI (*bottom*) and the WSO (*middle*). The thick black lines in the top panels are the heliospheric current sheet. The colored dots denote open field areas with positive polarity (*blue*) and negative polarity (*red*). The contours represent the magnetic field on the photosphere. The green contours represent the negative and the black contours the positive magnetic field.

November. The central meridian passage dates of the maps were, from top to bottom, September 4, October 1, October 28, and November 25. The magnetic field data were taken by the Michelson Doppler Imager (MDI) aboard the *Solar and Heliospheric Observatory* (*SOHO*; Scherrer et al. 1995). The CMEs in Table 1 occurred in the last two rotations. AR 10484 (*third panel*) actually appeared in the previous rotation but with a different active region number (AR 10464) and evolved until the following rotation (AR 10501). AR 10486 and 10488 emerged in the third rotation. AR 10498, a small active region, appeared in the third rotation, too. By reexamining the CMEs in Table 1, we can see that they were in fact associated with three active regions: AR 10484 (10501), 10486, and 10498.

3. RESULTS

3.1. *AR 10484 (10464, 10501) and the Large-Scale Magnetic Field*

Shown in Figure 2 are the locus of the computed heliospheric current sheet and the locations of the footpoints of open field lines that correspond to the locations of coronal holes (*top*), synoptic maps of the magnetic field taken by the Wilcox Solar Observatory (WSO) at Stanford University (*middle*), and by the *SOHO* MDI (*bottom*). The computation was done from the WSO synoptic maps based on the PFSS model. The thick black lines in the top panels represent the heliospheric current sheet that separates regions of opposite magnetic polarity; the dots are the locations of open field line footpoints in positive (*blue*) and negative (*red*) magnetic field regions. The contours represent the magnetic field on the photosphere, with green denoting negative and black denoting positive polarity. The left panels show the second rotation of Figure 1. AR 10464 has appeared by then. As a comparison, the data of the first rotation of Figure 1 (before the emergence of AR 10464) are shown on the right. It is seen that AR 10464 emerged in an open field area.

3.2. *AR 10486 and 10488 and the Large-Scale Magnetic Field*

The synoptic maps and the coronal field for the third rotation of Figure 1, when AR 10486 and 10488 have already emerged, are presented in Figure 3. Compared with the previous rotation when AR 10486 and 10488 did not appear (Fig. 2, *left*), it is clear that the active regions produced a large open field area after emerging.

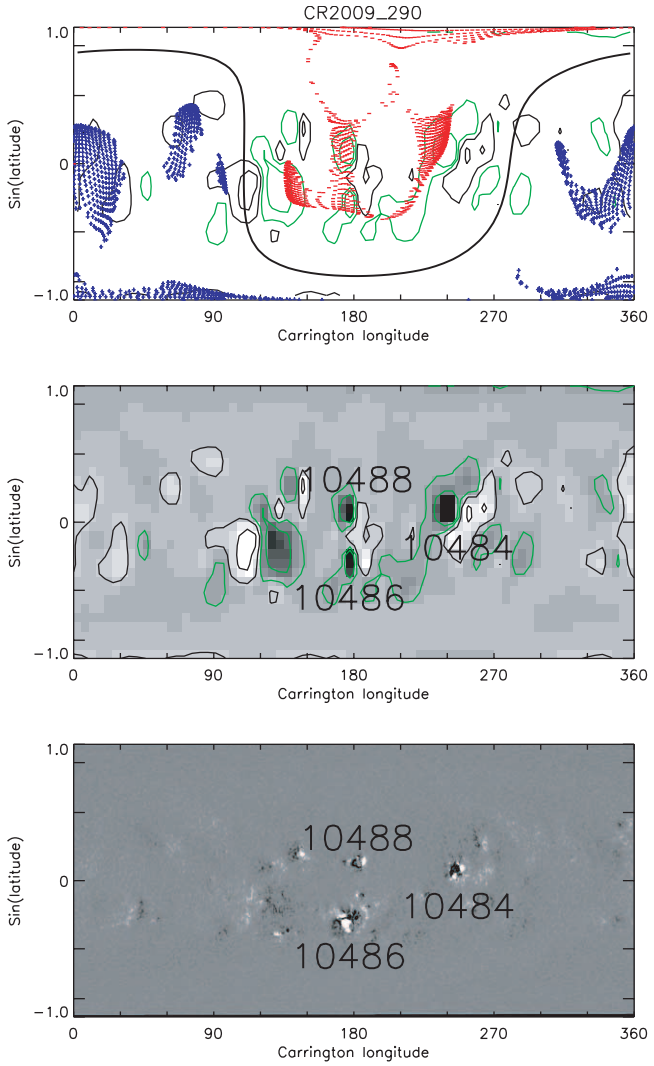

FIG. 3.—Same as Fig. 2, but for the third rotation of Fig. 1.

It is not surprising that some open magnetic flux emanates from the active regions. In fact, it has been shown, from observations and simulations, that open flux can also emerge from active regions (Levine et al. 1977; Svestka et al. 1977; Levine 1982; Kojima et al. 1999; Wang & Sheeley 2002; Luhmann et al. 2002; Neugebauer et al. 2002; Schrijver & DeRosa 2003; Liewer et al. 2004). Having performed simulations of active region emergence and the photospheric transport processes in the evolution of the open flux, Wang & Sheeley (2002) further argued that "emerging active regions act as sources of new open flux." Our calculation result agrees with their conclusion.

3.3. *AR 10498 and the Large-Scale Magnetic Field*

Unlike the active regions discussed in the previous sections, AR 10498 occurred fairly far from the open field areas. (See Fig. 4 [*left*]. The central meridian of the map denotes the 160° longitude of the Carrington rotation CR 2009.) In order to study the active region and the overlying magnetic field, we present in the right panels of Figure 4 the PFSS calculation in such a way that the magnetic configuration can be demonstrated in more detail: The dots in the top panel represent the footpoints of the open fields on the photosphere. The small bars denote closed field lines from positive polarity (*blue*) to negative polarity (*red*). The thick black line is the heliospheric current sheet. The colored lines in the middle panel represent the magnetic field lines starting from the boundaries of the open field areas on the photosphere to the source surface (defined as 2.5 $R_\odot$ by the PFSS model). These lines actually outline the open field areas from the solar surface to the source surface. The black line, again, is the heliospheric current sheet. The bottom panel shows the distribution of the magnetic field over the source surface. The colors here correspond to the open field areas on the solar surface. It is shown that AR 10498 is sitting at the boundary of two open field areas (Fig. 4, *bottom right, blue and green*) with the same polarity.

Such a configuration was first suggested by Hundhausen (1972) more than two decades ago, was observed by *Ulysses* and the *Advanced Composition Explorer* (*ACE*; Neugebauer et al. 2002), and was reproduced by Zhao & Webb (2003) using a PFSS model. By examining the *Ulysses* and *ACE* data, Neugebauer et al. (2002) reported the discovery of a boundary "between the plasmas from neighboring sources with the same polarity." Such a same-polarity source boundary is marked by a "plasma sheet" or "magnetic hole."

Neugebauer et al. (2004) further analyzed statistically the properties of the solar wind streams from such a configuration and compared them with the slow solar wind around the heliospheric current sheet (HCS). It was found that while they have many features in common, some dynamical properties of the wind near the same-polarity source boundary related regions differ from those near the HCS regions: greater minimum speed, smaller scale size, and lower peak and average density. Such characteristics of the solar wind from the same-polarity boundary (e.g., high background solar wind speed and low density) appear to be in favor of retaining the propagation speed of the disturbance.

3.4. *Summary of the Magnetic Configuration and the Fast Halo CMEs*

It has been demonstrated, from the evolution of the active regions and modeling the coronal magnetic field, that the active regions related to most (if not all) 2003 October–November fast halo CMEs were associated with special configurations of the magnetic field: The active regions were found to emerge within an open field area, produce a large open field area after emerging, or sit at the boundary of two open field areas with the same polarity.

It is not clear which role such configurations play in CMEs' initiation, but it is fairly apparent that they form an appropriate environment for propagation of the eruptions. This seems to imply that these structures helped at some level to ensure the high speed of the fast halo CMEs in 2003 October–November. In the following section, we carry out MHD simulations to explore the behavior of the propagation under the special structures of the background magnetic field and to quantitatively examine the influence of the special configurations.

4. MHD SIMULATION EXPERIMENTS

We carried out MHD simulations to examine how the magnetic field structure of the quiet corona influences the first phase of the CME propagation. The CME propagations were simulated as the responses of the numerically steady solar corona/wind to numerical perturbations.

To obtain the sub-Alfvénic steady corona, we first simulated the time relaxation of the sub-Alfvénic solar corona using the photospheric magnetic field map shown in the previous sections. The details of the MHD simulation code were described elsewhere

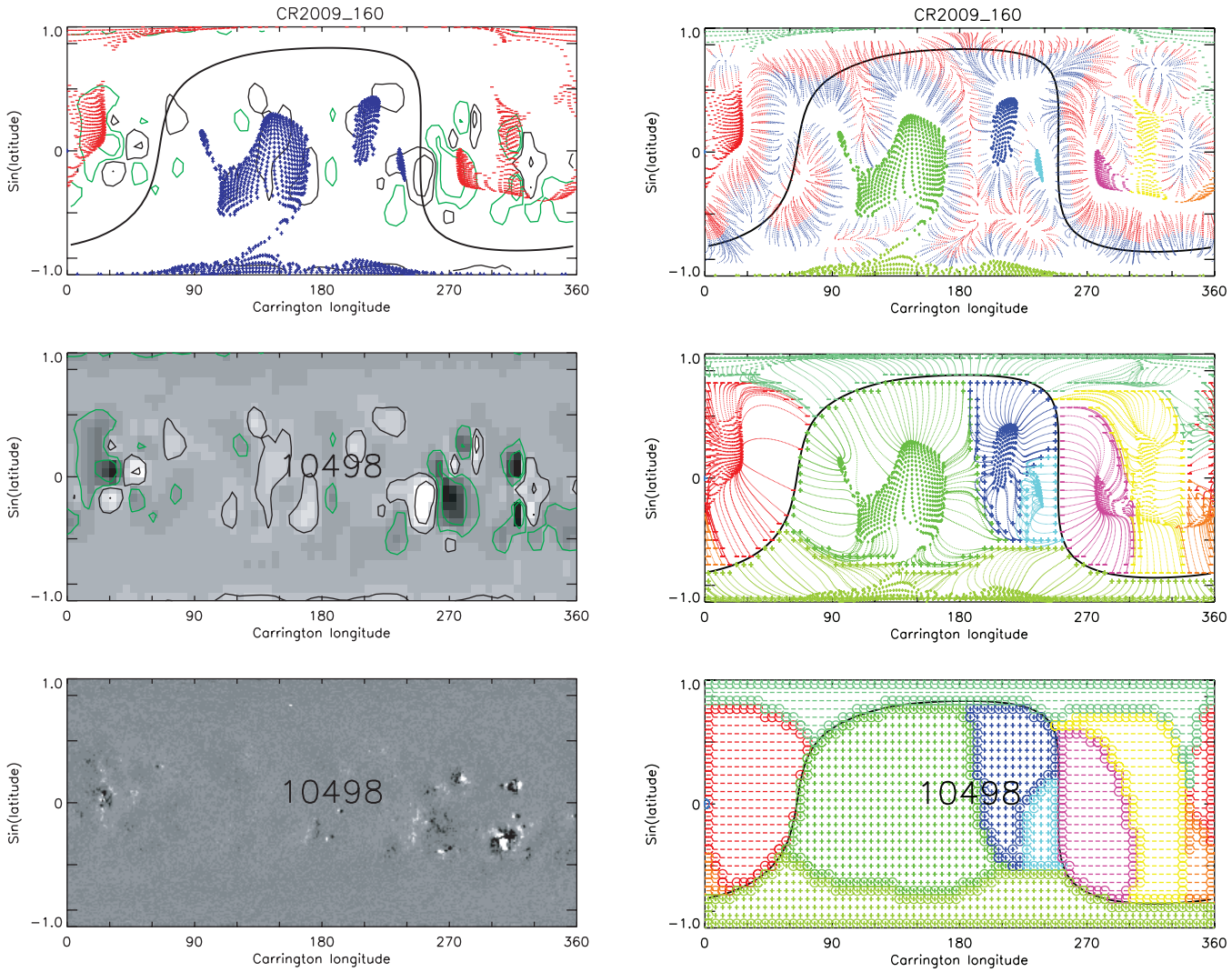

FIG. 4.—*Left:* Same as Fig. 2, but with the central meridian at 160° longitude of the Carrington rotation CR 2009. *Right:* Configuration of the coronal magnetic field calculated from a PFSS model. The dots in the top panel represent open field areas. The small bars denote closed field lines from positive polarity (*blue*) to negative polarity (*red*). The thick black line is the heliospheric current sheet. The colored lines in the middle panel represent the magnetic field lines starting from the boundaries of the open field areas on the photosphere to the source surface. The black line, again, is the heliospheric current sheet. The bottom panel shows the distribution of the magnetic field over the source surface. The colors here denote the corresponding open flux areas on the solar surface shown in the top panel.

(Hayashi 2005). A magnetic field computed from the PFSS model with the spherical harmonic coefficients up to the fifth term was used here as the initial and boundary values of the magnetic field.

To clarify and simplify the simulated situation, we only gave the increase of the mass density and pressure as the perturbation. Such perturbation allows us to avoid the complex process of the CME initiations, which are not well understood now. For fairness, the plasma velocity at the perturbation site was calculated so that the total momentum was preserved.

We chose to trace the flow speed discontinuity as a proxy for CME propagation because this discontinuity can be clearly defined. The gap between the density enhancement and the speed discontinuity is small in the region we examined (less than 5%–10% in heliocentric distance), and the profiles of their propagation speeds are quite similar.

We examined five cases, hereafter labeled A, B, C, X, and Y. For all cases, we used the same parameters except the latitude and longitude of the perturbation sites. The chosen altitude is 0.46 $R_\odot$ above the solar surface, the region of perturbation is a sphere with a diameter of 0.4 $R_\odot$, and the total mass and thermal energy are 8.6×10^{16} g and 5×10^{32} ergs, respectively. The total thermal energy is of the typical order of the magnetic energy released during the flare events.

4.1. *Propagation of the Perturbations and Open Magnetic Flux*

Two tests were performed to examine the behavior of the perturbation propagation when the open magnetic flux was present (like the events related to AR 10464 [10501] and AR 10486 and 10488, as described in §§ 3.1 and 3.2). We put an eruption in AR 10486 in the third rotation of Figure 1 (see also Fig. 3). We mark this test as case Y. As a comparison, we put the same eruption at the same location but in the previous rotation (the second rotation in Fig. 1, when AR 10486 and 10488 did not emerge) where no open flux was present (see Fig. 2, *right*). We call this test case X.

We plot in Figure 5 the distance of the shock front as a function of time. The curves marked X and Y represent cases X and Y. The simulation gives an average CME speed of 596 km s^{-1} for case X and 763 km s^{-1} for case Y. In other words, a CME's speed without the open flux present would have been only 78% of its speed with the open flux present.

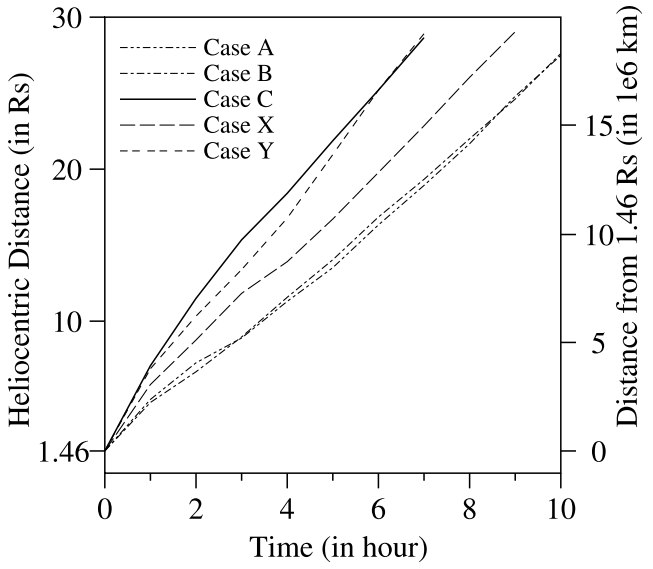

FIG. 5.—Positions of the shock fronts as a function of time for the five cases (see the text for details).

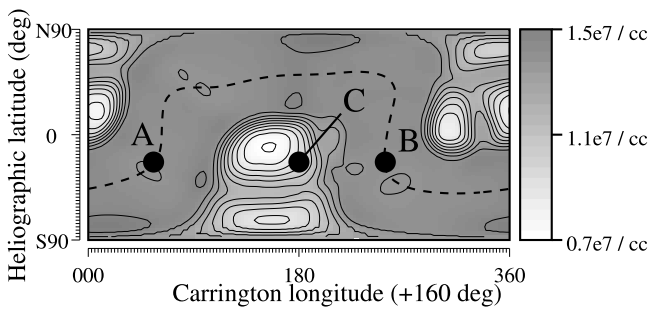

FIG. 6.—Background number density map at $r = 1.46\ R_{\odot}$. A, B, and C denote the positions where the numerical perturbations were given.

4.2. *Propagation of Perturbations along Current Sheet and Plasma Sheet*

The other three tests, cases A, B, and C, were carried out to investigate the behavior of the perturbation propagation with the presence of current sheets or plasma sheets. We put three eruptions in the synoptic map shown in the left panels of Figure 4. The eruptions in cases A and B are under a heliospheric current sheet, while the eruption in case C is under a plasma sheet (see Fig. 6), where AR 10498 was sitting (see also Fig. 4).

The curves marked A, B, and C in Figure 5 represent the distances of the shocks as a function of time for cases A, B, and C. The average speeds from the simulations are 506 km s^{-1} for case A, 509 km s^{-1} for case B, and 755 km s^{-1} for case C. It is evident that the speeds for cases A and B are much lower than that for case C (only 67% of the speed for case C).

4.3. *Summary of MHD Simulation*

The propagations of the coronal disturbances in the post-CME phase were simulated by giving the numerical density and temperature enhancement and tracing the response of the solar corona. The behavior of the propagations has been compared with different configurations of the magnetic field in the background. It is demonstrated that when an active region is within an open flux area (like AR 10464, which emerged in the open flux area, or AR 10486 and 10488, which produced a large open flux area after they emerged), the related CMEs are faster than those without open flux. It is also shown that the propagation of a disturbance under a plasma sheet could be much faster than that under a current sheet. Therefore, it is suggested that the magnetic field configuration in the background, as found in our PFSS model in the previous sections and simulated here in this section, is an additional factor that influences coronal disturbance propagation.

5. CONCLUSIONS AND DISCUSSION

We have analyzed most (if not all) fast halo CMEs in 2003 October–November in terms of the configuration of the large-scale magnetic field. The observations and modeling have demonstrated that the large-scale magnetic field associated with these CMEs possesses special configurations: open magnetic flux or a plasma sheet. Such configurations appear to be in favor of propagation of the disturbances.

We have also carried out MHD simulations to quantitatively examine the influence of the special magnetic configurations for the CMEs' propagation. The experiments suggest that propagation with the presence of open flux is faster than that without open flux present and that CMEs occurring under a plasma sheet travel much faster than those under a heliospheric current sheet.

Several flare-related CMEs, observed from multiple wavelengths by various instruments, have been presented recently to illustrate their kinematic evolution from the solar surface to the heliosphere and interplanetary space (e.g., Zhang et al. 2001; Alexander et al. 2002; Neupert et al. 2001; Moon et al. 2002; Yurchyshyn 2002; Gallagher et al. 2003; Shanmugaraju et al. 2003). It is evident that those CMEs demonstrated a common kinematic behavior: first being impulsively accelerated near the solar surface and then moving outward at fairly constant speeds. Zhang et al. (2001) further suggested three phases in the CME kinematic evolution: (1) initial phase, (2) impulsive acceleration phase, and (3) gradual phase. This seems to imply that processes near the solar surface play an important role in determining the speed of a CME. Recently, many pieces of work were presented to show that the acceleration of a flare-related CME is probably determined by the magnitudes of the associated flares and/or the rate of magnetic reconnection during flares (see, e.g., Moon et al. 2002; Cheng et al. 2003; Zhang et al. 2004; Qiu et al. 2004; Jing et al. 2005).

While it is likely that the speed of a flare-related CME is primarily determined by the characteristics of the associated flare, it is still interesting to investigate the role that the associated large-scale field plays to shape the kinematic behavior of the CME. In fact, Chen (1996) has demonstrated the effect of the overlying field over a modeled flux rope that was erupted due to injection of the poloidal flux into the system. It is shown in that work that when the flux rope moved upward after eruption, the major forces withholding the motion were the Lorentz force from the toroidal current and the background field and gravity (Fig. 7 in that paper). Thus, strong closed flux in the background field may function to slow down the CME or even pull back the eruptive materials, leading to failure of the eruptions. For example, Ji et al. (2003) observed a failed eruption of a filament. The filament first erupted, causing an M2 class flare, and then fell back to the solar surface, unable to lead to a CME. They suggested that the eruption failed because the event was not able to break out of the field crossed over the filament, so those closed fields pulled the filament back by magnetic tension.

It is thus suggested that configurations of the background magnetic field such as those illustrated in this paper may have worked as an additional condition to ensure the high speed of

the fast halo CMEs in 2003 October–November. It needs to be pointed out, however, that since we did not examine more cases for the fast halo CMEs, we cannot reach a general conclusion that such special configurations are common structures applicable to all fast halo CMEs. A statistical study is needed.

We wish to thank the anonymous referee for useful comments and suggestions, which led to reorganization of the paper and better presentation of the results. We thank X. Zhao at Stanford University for providing the PFSS code. We appreciate Seiji Yashiro, Grzegorz Michalek, and Nat Gopalswamy for compiling the *SOHO* LASCO CME catalog, which is generated and maintained by NASA and the Catholic University of America in cooperation with the Naval Research Laboratory. This work was supported by NASA grant NAG5-13261, the NSF CISM project under grant ATM 01-20950, and DOD MURI grants. *SOHO* is a project of international cooperation between ESA and NASA.

REFERENCES

Alexander, D., Metcalf, T. R., & Nitta, N. 2002, Geophys. Res. Lett., 29, 13670
Altschuler, M. D., & Newkirk, G. 1969, Sol. Phys., 9, 131
Arge, C. N., & Pizzo, V. J. 2000, J. Geophys. Res., 105, 10465
Chen, J. 1996, J. Geophys. Res., 101, 27499
Cheng, C. Z., Ren, Y., Choe, G. S., & Moon, Y. J. 2003, ApJ, 596, 1341
Gallagher, P. T., Lawrence, G. R., & Dennis, B. R. 2003, ApJ, 588, L53
Gopalswamy, N., Barbieri, L., Cliver, E. W., Lu, G., Plunkett, S. P., & Skoug, R. M. 2005a, J. Geophys. Res., 110, 011268
———. 2005b, Geophys. Res. Lett., 32, 022348
Gopalswamy, N., Yashiro, S., Liu, Y., Michalek, G., Vourlidas, A., Kaiser, M. L., & Howard, R. A. 2005c, J. Geophys. Res., 110, 010958
Hayashi, K. 2005, ApJS, 161, 480
Hoeksema, J. T., Wilcox, J. M., & Scherrer, P. H. 1982, J. Geophys. Res., 87, 10331
Hundhausen, A. J. 1972, Coronal Expansion and Solar Wind (New York: Springer)
Ji, H., Wang, H., Schmahl, E. J., Moon, Y.-J., & Jiang, Y. 2003, ApJ, 595, L135
Jing, J., Qiu, J., Lin, J., Qu, M., Xu, Y., & Wang, H. 2005, ApJ, 620, 1085
Kojima, M., Fujiki, K., Ohmi, T., Tokumaru, M., Yokobe, A., & Hakamada, K. 1999, J. Geophys. Res., 104, 16993
Levine, R. H. 1982, Sol. Phys., 79, 203
Levine, R. H., Altschuler, M. D., Harvey, J. W., & Jackson, B. V. 1977, ApJ, 215, 636
Liewer, P. C., Neugebauer, M., & Zurbuchen, T. 2004, Sol. Phys., 223, 209
Luhmann, J. G., Li, Y., Arge, C. N., Gazis, P. R., & Ulrich, R. 2002, J. Geophys. Res., 107, 101029
Metcalf, T. R., Leka, K. D., & Mickey, D. L. 2005, ApJ, 623, L53
Moon, Y.-J., Choe, G. S., Wang, H., Park, Y. D., Gopalswamy, N., Yang, G., & Yashiro, S. 2002, ApJ, 581, 694
Neugebauer, M., Liewer, P. C., Goldstein, B. E., Zhou, X., & Steinberg, J. T. 2004, J. Geophys. Res., 109, 10102
Neugebauer, M., Liewer, P. C., Smith, E. J., Skoug, R. M., & Zurbuchen, T. H. 2002, J. Geophys. Res., 107, 1488
Neupert, W. M., Thompson, B. J., Gurman, J. B., & Plunkett, S. P. 2001, J. Geophys. Res., 106, 25215
Qiu, J., Wang, H., Cheng, C. Z., & Gary, D. E. 2004, ApJ, 604, 900
Schatten, K. H., Wilcox, J. M., & Ness, N. F. 1969, Sol. Phys., 6, 442
Scherrer, P. H., et al. 1995, Sol. Phys., 162, 129
Schrijver, C. J., & DeRosa, M. L. 2003, Sol. Phys., 212, 165
Shanmugaraju, A., Moon, Y.-J., Dryer, M., & Umapathy, S. 2003, Sol. Phys., 215, 185
Svestka, Z., Solodyna, C. V., Howard, R., & Levine, R. H. 1977, Sol. Phys., 55, 359
Wang, Y.-M. 1993, J. Geophys. Res., 98, 3529
Wang, Y.-M., & Sheeley, N. R., Jr. 1990, ApJ, 355, 726
———. 1992, ApJ, 392, 310
———. 2002, J. Geophys. Res., 107, 1302
Xu, Y., Cao, W., Liu, C., Yang, G., Qiu, J., Jing, J., Denker, C., & Wang, H. 2004, ApJ, 607, L131
Yang, G., Xu, Y., Cao, W., Wang, H., Denker, C., & Rimmele, T. R. 2004, ApJ, 617, L151
Yurchyshyn, V. B. 2002, ApJ, 576, 493
Zhang, J., Dere, K. P., Howard, R. A., Kundu, M. R., & White, S. M. 2001, ApJ, 559, 452
Zhang, J., Dere, K. P., Howard, R. A., & Vourlidas, A. 2004, ApJ, 604, 420
Zhao, X. P., & Webb, D. F. 2003, J. Geophys. Res., 108, 101029